Spectroscopy of transmission resonances through a C60 junction

Schneider, N. L.; Néel, N.; Papior, Nick Rübner; Lu, Jing Tao; Brandbyge, Mads; Kröger, J.; Berndt, R.

Published in:
Journal of Physics: Condensed Matter

Link to article, DOI:
10.1088/0953-8984/27/1/015001

Publication date:
2015

Document Version
Publisher's PDF, also known as Version of record

Spectroscopy of transmission resonances through a C_{60} junction

2015 J. Phys.: Condens. Matter 27 015001

(http://iopscience.iop.org/0953-8984/27/1/015001)

OPEN ACCESS
IOP Publishing
Journal of Physics: Condensed Matter
J. Phys.: Condens. Matter **27** (2015) 015001 (6pp)
doi:10.1088/0953-8984/27/1/015001

Spectroscopy of transmission resonances through a C_{60} junction

N L Schneider[1], N Néel[1], N P Andersen[2], J T Lü[2,3], M Brandbyge[2], J Kröger[4] and R Berndt[1]

[1] Institut für Experimentelle und Angewandte Physik, Christian-Albrechts-Universität zu Kiel, D-24098 Kiel, Germany
[2] DTU Nanotech, Technical University of Denmark, Anker Engelunds Vej 1 Bygning 101A, DK-2800 Kongens Lyngby, Denmark
[3] School of Physics, Huazhong University of Science and Technology, Wuhan, China
[4] Institut für Physik, Technische Universität Ilmenau, D-98693 Ilmenau, Germany

E-mail: joerg.kroeger@tu-ilmenau.de

Received 12 August 2014, revised 11 October 2014
Accepted for publication 24 October 2014
Published 19 November 2014

Abstract

Electron transport through a single C_{60} molecule on Cu(1 1 1) has been investigated with a scanning tunnelling microscope in tunnelling and contact ranges. Single-C_{60} junctions have been fabricated by establishing a contact between the molecule and the tip, which is reflected by a down-shift in the lowest unoccupied molecular orbital resonance. These junctions are stable even at elevated bias voltages enabling conductance measurements at high voltages and nonlinear conductance spectroscopy in tunnelling and contact ranges. Spectroscopy and first principles transport calculations clarify the relation between molecular orbital resonances and the junction conductance. Due to the strong molecule–electrode coupling the simple picture of electron transport through individual orbitals does not hold.

Keywords: scanning tunnelling microscopy, scanning tunnelling spectroscopy, single-molecule junction, transport calculation

(Some figures may appear in colour only in the online journal)

1. Introduction

The transport of electrons through atomic-scale contacts between two electrodes may be interpreted in terms of transport channels—quantum states extending between the electrodes—and their transmission probabilities τ_n [1]. In calculations, these probabilities vary drastically as a function of the electron energy [2–5]. Experiments have addressed the low-bias conductance [2, 6–14] and therefore typically provided little information on the transport channels and their τ_n. Metallic contacts between superconducting leads are a notable exception. In this case, Andreev reflections have been used to experimentally determine the τ_n at low bias [2, 6, 7]. However, experimental data on the variation of τ_n with the electron energy E were not reported.

Molecular junctions are expected to exhibit more and sharper structure of $\tau_n(E)$ [15]. The energy gap between occupied and unoccupied states of many molecules used in contact experiments is of the order of electron volts. As a result, probing their contributions to the conductance at contact is difficult. At the required elevated voltages and correspondingly large currents heating of the junctions occurs [16–19] and may lead to their destruction [17]. In a previous break-junction experiment the number of transport channels in benzene junctions has been determined using shot noise measurements [20]. To date, hardly any experimental data are available for highly conductive molecular junctions [20, 21].

Here, we report results from single-molecule contacts to C_{60} on Cu(1 1 1). Owing to a C_{60}-induced reconstruction the contacts are stable enough for conductance spectroscopy $[G(V)]$ at elevated bias voltages. Conductance resonances are observed and quantitatively analyzed using first-principles calculations. As expected, the molecular orbitals leave their

footprint on $G(V)$. However, it turns out that a picture of parallel transport through individual orbitals is too simple and only accounts for a fraction of the total conductance.

2. Experiment

Experiments were performed with a scanning tunnelling microscope (STM) operated at 8 K and in ultrahigh vacuum with a base pressure of 10^{-9} Pa. Chemically etched W tips and Cu(1 1 1) surfaces were cleaned by Ar^+ bombardment and annealing. C_{60} molecules were sublimated from a Ta crucible and adsorbed to clean Cu(1 1 1) at room temperature. After C_{60} deposition the surface was annealed at 500 K for 10 min. This preparation leads to the formation of well ordered C_{60} islands and a reconstruction of the Cu(1 1 1) surface [22]. To form a single-molecule contact the STM tip was brought closer towards the center of a molecule and the current was simultaneously recorded. Before and after contact experiments STM images and spectra of the differential conductance ($\mathrm{d}I/\mathrm{d}V$) were recorded to detect tip or molecule modifications. It turned out that the junctions are stable up to currents of ≈20 μA at elevated voltages of ≈1 V. Spectroscopy of $\mathrm{d}I/\mathrm{d}V$ was performed by modulating the sample voltage (10 $\mathrm{mV_{rms}}$, 8 kHz) and measuring the current response with a lock-in amplifier.

3. Theory

To simulate experimental data, tunnelling and contact junctions were modelled by a tetrahedral Cu tip attached to a 4 × 4 surface unit cell in a 7-layer Cu slab (substrate) and a C_{60} molecule adsorbed with a C hexagon to an on-top Cu(1 1 1) site (inset to figure 3(*b*)). The electronic structure, contact formation and conductance of the C_{60} junction were calculated within density functional theory (DFT) with the generalized gradient approximation (GGA-PBE) [23] to the exchange-correlation functional and a 2 × 2 surface k-point sampling. A localized atomic orbital basis set (SIESTA) [24] as well as a plane-wave basis set (VASP) [25] were used in order to access and avoid basis set superposition errors, which are present in calculations based on the linear combination of atomic orbitals. A series of calculations were performed in which the tip and the surface were approached towards each other in steps of 0.1 Å by decreasing the unit cell dimension in the approach direction. Relaxations of the tip tetraeder, the C_{60} molecule, and the two outermost surface layers were considered in these calculations. The TRANSIESTA [26] method was then applied to perform transport calculations of the linear conductance as well as non-equilibrium calculations of the current–voltage characteristics for two selected junction configurations in the tunnelling and contact range.

4. Results and discussion

The inset to figure 1 shows a constant-current STM image from the interior of a C_{60} island. Similar to previous observations from other surfaces [27–30], the molecules exhibit three protrusions, which are due to the next-to-lowest unoccupied

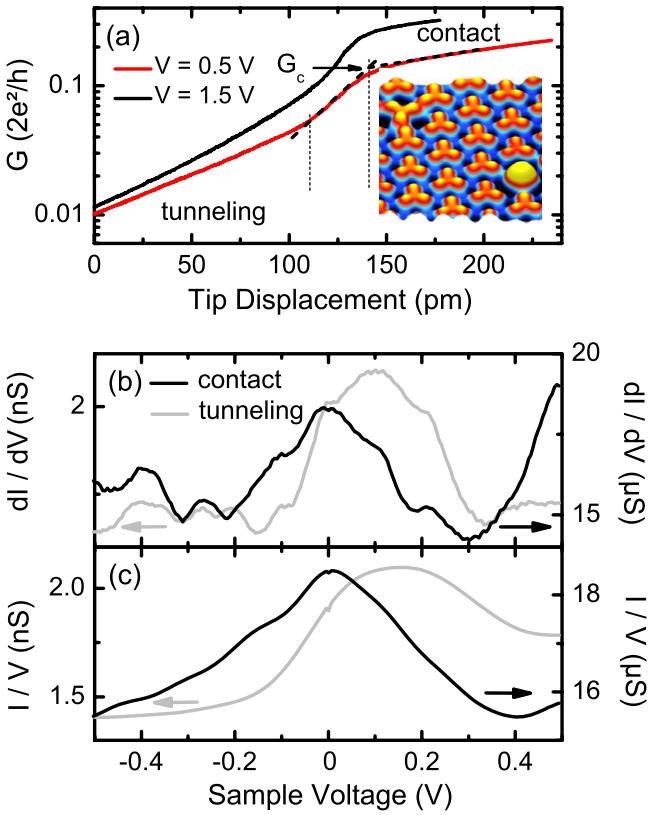

Figure 1. (*a*) Conductance of C_{60} on Cu(1 1 1) in a STM versus displacement of the tip towards the molecule. Red and black lines indicate data recorded at sample voltages $V = 0.5$ V and 1.5 V, respectively. Dashed lines illustrate the definition of the point of contact formation and the corresponding conductance G_c. Vertical lines separate different conductance ranges, namely tunnelling, transition, and contact. Inset: pseudo-three-dimensional representation of a constant-current STM image of a C_{60} monolayer on Cu(1 1 1) (1.5 V, 100 pA, 6 × 6 $\mathrm{nm^2}$). (*b*) $\mathrm{d}I/\mathrm{d}V$ and (*c*) I/V curves as a function of V acquired at fixed tip heights in the tunnelling range (grey) and at contact (black). Tip heights were set by disabling the STM feedback loop at 0.6 V and, respectively, 0.7 nA and 11.6 μA in tunnelling and contact ranges. The small sharp feature at $V = 0$ in (*c*) is a numerical artefact.

molecular orbital (LUMO+1). This orbital is centred at the three C pentagons that surround a hexagon in the observed trifoliate way. When the tip is brought closer to a molecule the conductance varies as displayed in figure 1(*a*). Tunnelling, transition and contact ranges are defined using the intersections of exponential fits to the conductance data (indicated in the lower curve of figure 1(*a*)) [31]. The two data sets shown were recorded at sample voltages $V = 0.5$ V and 1.5 V and exhibit different conductances G_c at the transition to contact, namely ≈0.15 G_0 and ≈0.25 G_0, respectively.

To relate the bias dependence of the conductance to the electronic structure of the adsorbed molecule, $\mathrm{d}I/\mathrm{d}V$ spectra were acquired at constant tip–sample separations. The grey and black lines in figure 1(*b*) show data sets from the tunnelling and contact ranges, respectively. In the tunnelling range constant-height $\mathrm{d}I/\mathrm{d}V$ spectra of C_{60} can be routinely recorded over a fairly wide range of bias voltages. At contact, however, currents on the order of 10 μA flow and the junction usually becomes unstable at much lower voltages. Owing to

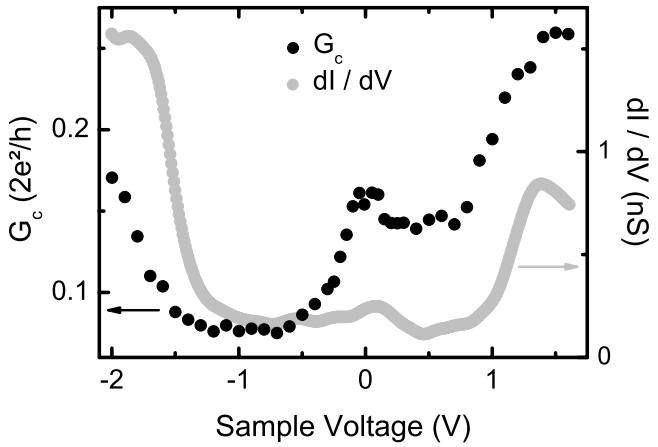

Figure 2. Contact conductance G_c (black) and tunnelling $\mathrm{d}I/\mathrm{d}V$ data (grey) versus sample voltage. G_c has been extracted from individual conductance-versus-displacement curves (see figure 1(*a*)) acquired at voltages between −2 V and 1.6 V.

the particular stability of the structures used here, the range from −0.5 to 0.5 V can be probed. The tunnelling data of figure 1(*b*) show a peak centred at ≈100 mV. Previous reports have shown that it is due to the C_{60} LUMO [22, 32]. At contact, a similar peak is observed, albeit broadened and shifted to ≈0 mV. Our calculations (*vide infra*) reveal a hybridization of C_{60} with the tip. It is not clear that the contact data may simply be interpreted in terms of a density of states of the junction. Ignoring this issue for the moment, we find that the differences of the contact spectrum are consistent with the calculated electronic structure of the junction. Figure 1(*c*) shows the conductances $G = I/V$, which were recorded along with the $\mathrm{d}I/\mathrm{d}V$ spectra.

To extend the accessible range of voltages at contact, a different method was used. Rather than sweeping the voltage at a fixed tip–molecule distance, the current was recorded as a function of the tip height while keeping V fixed. The conductance G_c at contact formation was then extracted as described above (figure 1). The results are depicted in figure 2 (black) together with a constant-height tunnelling $\mathrm{d}I/\mathrm{d}V$ spectrum (grey). Over the investigated voltage range $-2\,\mathrm{V} \leqslant V \leqslant 1.6\,\mathrm{V}$, the contact conductance G_c varies significantly between $0.07\,G_0$ and $0.26\,G_0$. Moreover, the maxima at $V \approx 0\,\mathrm{V}$ and ≈1.5 V) are close to maxima of the tunnelling $\mathrm{d}I/\mathrm{d}V$ data at ≈100 mV (LUMO) and ≈1.3 V (LUMO+1).

DFT calculations based on the structure shown in the inset to figure 3(*b*) were performed to rationalize the experimentally observed shift of the LUMO resonance to lower energies upon the tunnelling-to-contact transition. Figure 3 shows the zero-bias transmission functions calculated with a 9 × 9 surface k-point sampling. The peak-like structure close to the Fermi energy (E_F) is due to the LUMO resonance, which clearly shifts towards E_F upon decreasing tip–C_{60} distances and thus increasing hybridization. According to a Bader charge analysis based on the VASP calculations [33] a charge of ≈0.4 e is transferred from the tip to the molecule. For large tip–molecule distances in the tunnelling range the transmission function exhibits an approximate exponential variation with

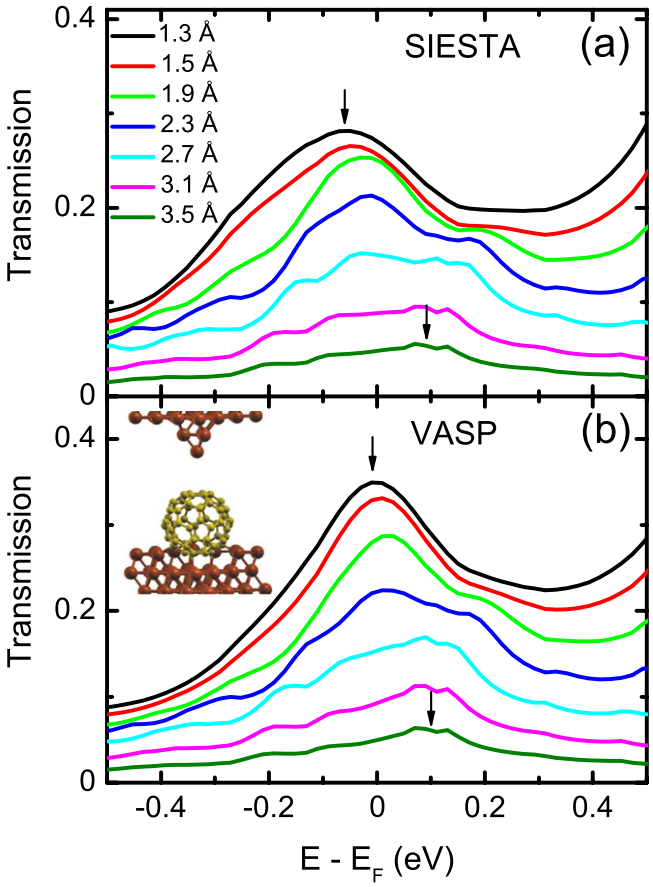

Figure 3. Transmission functions calculated using relaxed geometries obtained from SIESTA (*a*) and VASP (*b*) with PBE-GGA labelled by the unrelaxed tip–C_{60} distances measured from the tip apex atom to the C hexagon plane. Beyond contact formation at 1.7 Å (unrelaxed distance) the relaxed tip–C_{60} distance hardly changes. Instead the tip is progressively compressed in both SIESTA and VASP calculations. The transmission functions show the change of the C_{60} LUMO resonance close to the Fermi energy (E_F) at zero bias during contact formation. A clear lowering of the resonance energy towards E_F is observed (vertical arrows). The functional form of the transmission versus energy roughly shows an exponential decrease in magnitude with increasing tip–C_{60} distance in the tunnelling range starting from ≈2.7 Å. The inset to (*b*) shows the structural model of the junction used in the calculations.

the distance. The contact formation may be observed as a deviation from this scaling behaviour due to the onset of chemical interactions leading to a resonance shift and broadening. Such deviations are indeed present for a tip–hexagon distance between 2.3 and 2.7 Å with a corresponding conductance of $\approx 0.2\,G_0$. According to the experiments the contact conductance close to zero bias voltage is $\approx 0.16\,G_0$ (figure 2). For tip–molecule distances at which repulsive interactions start to deform the tip apex into a flat geometry the conductance is close to $0.3\,G_0$. At positive energies, starting from ≈0.4 eV the tail of a second transmission resonance has been observed in the calculations (figure 3).

Figure 3 compares results using geometries obtained from SIESTA (figure 3(*a*)) and VASP PBE-GGA (figure 3(*b*)) calculations. Both methods lead to virtually identical evolutions of the energy-dependent transmission functions. In the SIESTA calculations the tip apex atom is slightly

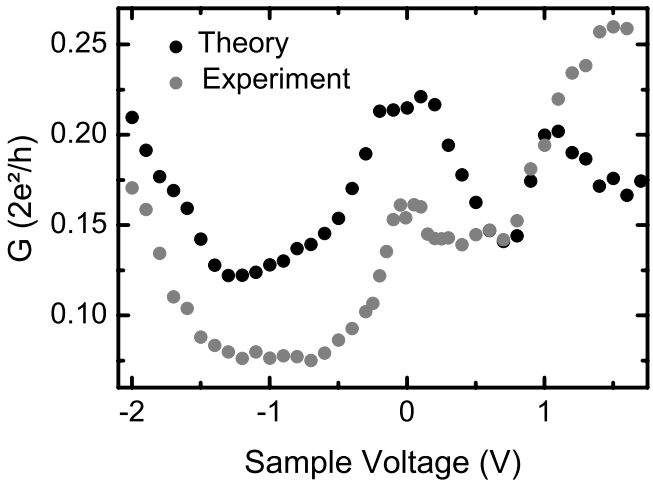

Figure 4. Comparison of experimental G_c (grey) and calculated conductances (black). In the calculations the tip apex atom was separated by 2 Å from the closest C_{60} hexagon.

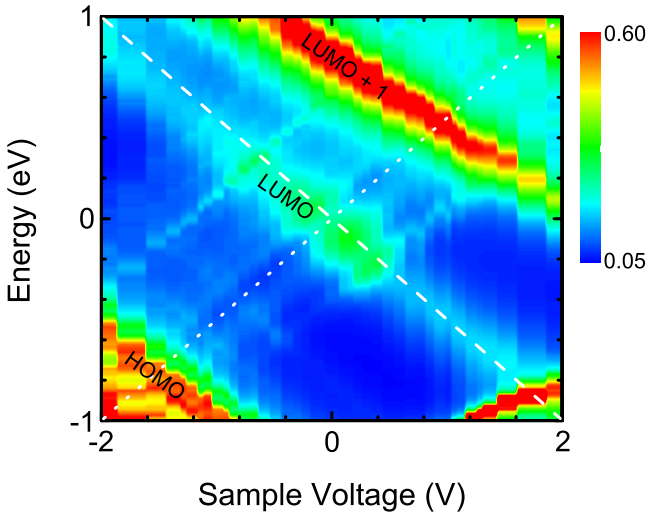

Figure 5. Density plot of the transmission function, $T(E, V) = \sum_n \tau_n(E, V)$, for different energies E and voltages V in the contact range. The energies of the transmission maxima labelled HOMO, LUMO, and LUMO+1 approximately follow the chemical potential of the sample $-eV/2$ (dashed line). Weaker transmission features are related to tip states and follow the chemical potential of the tip ($+eV/2$, dotted line).

stretched towards the C_{60} molecule upon approaching the tip to the surface. Further approach of the tip leads to a repulsive tip–molecule interaction and deforms the tip apex towards a flat geometry. Including van der Waals forces in the VASP calculations [34] (not shown) did not lead to markedly different conductance behaviour with tip displacement. While the calculated conductances in the contact range are in good agreement with the experimentally observed values, the calculated exponential variation of the conductance with the tip–molecule distance in the tunnelling range is somewhat larger than in the experiments. This observation is probably due to the use of an atomic basis set description of the tip [35]. In addition, as is evident from figure 1(*a*) the slope of conductance-displacement characteristics depends on the bias voltage both in tunnelling and contact ranges. Thus, the bias voltage plays a significant role in the effective tunnelling barrier as well as in the contact formation. This effect could likewise involve bias voltage-induced atomic relaxations. In the calculations we neglect the computationally very demanding bias-induced relaxations but note that these can lead to significant forces in the contact range [19].

Next, full non-equilibrium calculations based on the junction geometries obtained from SIESTA were performed. The resulting bias voltage-dependent conductances at contact in figure 4 (black) displays much similarity with the experimental data (grey). A resonance with ≈1 V full width at half maximum is centred around 0 V. In addition, resonances are observed in the calculations for negative and positive bias voltages, which are similar to the experimental results.

Figure 5 shows how these transmission maxima change with the sample voltage. As expected from the strong C_{60}–Cu(1 1 1) coupling, the maxima essentially follow the sample chemical potential, which is defined as $-eV/2$ with V the sample voltage. Slight deviations from the evolution of the sample chemical potential are due to a small coupling between the molecule and the tip. As exposed in detail next, the notion of individual molecular states and their identification with transmission maxima requires some caution due to the strong molecule–electrode coupling. Allowing only transport via the highest occupied molecular orbital (HOMO), LUMO, or LUMO+1 states of the molecular region in the calculation does indeed warrant this designation. However, the simple picture of parallel transport via each of these orbitals only accounts for a fraction of the total transmission, as demonstrated below.

The standard Green function expression [26] for the elastic transmission, T, reads

$$T(E) = \mathrm{Tr}\left[G(E)\Gamma_{\mathrm{L}}(E)G^{\dagger}(E)\Gamma_{\mathrm{R}}(E)\right], \qquad (1)$$

where G is the retarded Green function matrix and $\Gamma_{\mathrm{L/R}}$ the electrode coupling matrices in the full basis set describing the scattering region. The transmission eigenchannels τ_n, with $T(E) = \sum_n \tau_n(E)$ (figure 6(*a*)) [15], provide an exact decomposition of the total transmission, but do typically not show a separation into molecular orbitals. The dominant transmission eigenchannel (black line in figure 6(*a*), transmission probability $\tau_1(E)$) closely follows the C_{60} HOMO, LUMO, and LUMO+1. The single channel giving rise to the LUMO transmission is due to the coupling of the rotational symmetric s orbital on the tip around the Fermi energy. Close to the LUMO+1 energy (≈0.9 eV) three channels contribute to the conductance.

To test whether transport takes place in parallel via molecular orbitals of C_{60} the eigenstates of the molecule-projected self-consistent Hamiltonian (MPSH) [36] were calculated, which correspond to the HOMO, LUMO, and LUMO+1. The coupling matrices in equation (1) were then projected onto each of these orbitals in order to evaluate the transmission probability of electrons that enter and exit the C_{60} junction via one of these orbitals. The projected electrode couplings read $\Gamma^{\alpha}_{\mathrm{L/R}} = P_{\alpha}\Gamma_{\mathrm{L/R}}P_{\alpha}$, where α is one of the molecular orbitals and P_{α} a corresponding projector

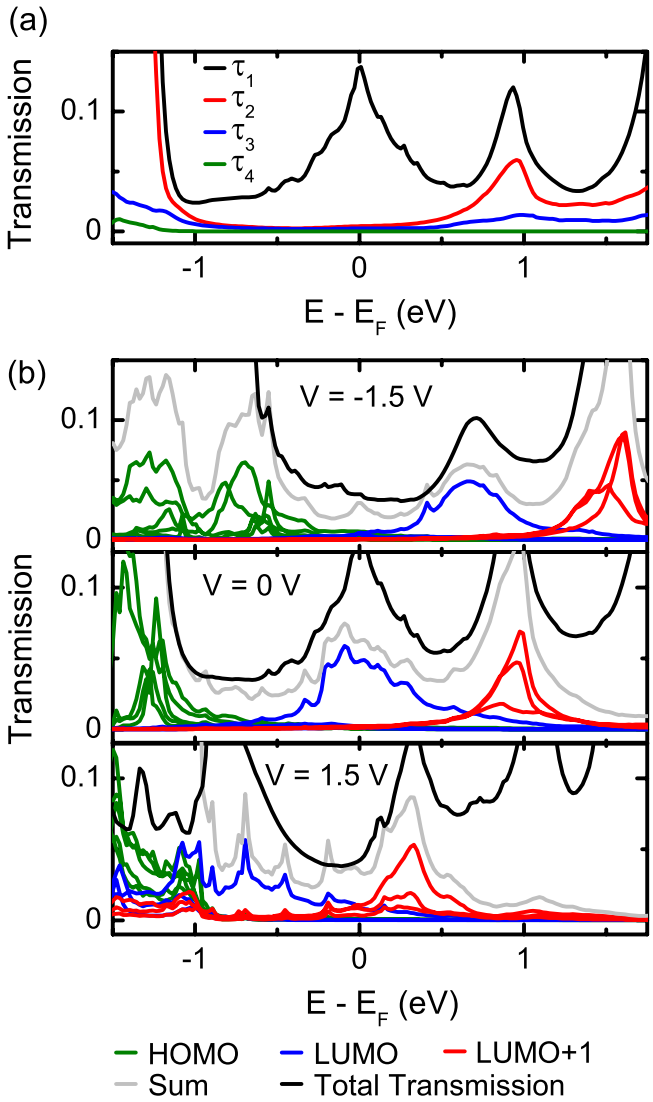

Figure 6. (*a*) Eigenchannel transmissions, $\tau_n(E)$ ($n = 1, \ldots, 4$), at zero bias for the contact range (tip–C_{60} distance: 1.9 Å) averaged over all k points. The dominant transmission channel (black, transmission probability $\tau_1(E)$) closely follows the C_{60} HOMO, LUMO, and LUMO+1. Around the energy of the LUMO+1 (≈0.9 eV) three channels contribute to the conductance. (*b*) Orbital-projected transmission functions $T_\alpha(E)$ for the C_{60} HOMO (green), LUMO (blue) and LUMO+1 (red) resonances evaluated at the indicated voltages (tip–C_{60} distance: 1.9 Å, i.e. in the contact range). Several contributions are observed from each orbital due to their partial degeneracy. The grey line depicts the sum of all transmissions, $\sum_\alpha T_\alpha(E)$, while the solid black line is the total transmission calculated according to equation (1).

for the same subset region. Using $\Gamma^\alpha_{L/R}$ in equation (1) the resulting T_α,

$$T_\alpha(E) = \mathrm{Tr}\left[G(E)\Gamma^\alpha_L(E)G^\dagger(E)\Gamma^\alpha_R(E)\right], \qquad (2)$$

is interpreted as the electron transmission via orbital α. Therefore, $T_\alpha(E)$ may be used to judge the extent to which the assignment of individual orbitals to a specific transmission feature is valid. Figure 6(*b*) shows the k-averaged transmission functions $T_\alpha(E)$ for the HOMO (green), LUMO (blue) and the LUMO+1 (red) at bias voltages of −1.5 V (top), 0 V (middle),

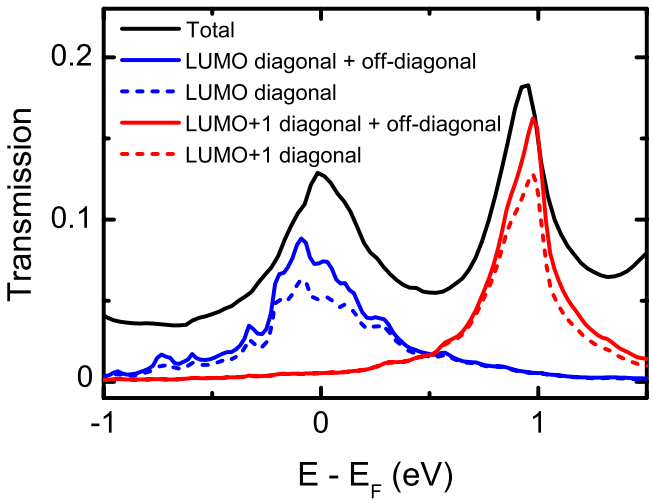

Figure 7. Contributions to LUMO and LUMO+1 transmissions from diagonal (dashed lines) terms (α = LUMO, LUMO + 1 in equation (2)), and off-diagonal/mixing (full lines) contributions to the LUMO, LUMO+1 transmission from nearby orbitals (HOMO, LUMO, LUMO+1) (equation (3)).

+1.5 V (bottom). The fivefold (threefold) degeneracy of the HOMO (LUMO, LUMO+1) of the free C_{60} molecule is partly lifted for C_{60} attached to the electrodes. Each degenerate orbital contributes to the transmission. The sum of all transmission curves is plotted as a grey line.

It is clear from figure 6(*b*) that the projected transmissions of the HOMO, LUMO, and LUMO+1 do indeed follow the main peaks in the total transmission. The shift of individual transmission peaks to lower energies with increasing bias voltage (figure 5) is also visible. However, the projected transmissions of HOMO, LUMO, LUMO+1 do not add up to the total transmission (black line in figure 6(*b*)) in the energy range where we expect the conductance to take place in these. Mostly the sum of projected transmissions (grey line) is lower than the total transmission (black line)[4]. In figure 6(*b*) we have restricted the calculations to the HOMO, LUMO and LUMO+1. It is necessary to include more molecular orbitals in the sum to obtain peaks farther from E_F. For instance, in figure 6(*b*) the total transmission peaks for energies exceeding 1 eV cannot be accounted for by the contributions from the chosen projected orbitals (grey line) and would require inclusion of the LUMO+2. For obtaining the full picture the off-diagonal contributions from different α in equation (2) must be considered. Electrons enter and exit the molecule via different orbitals α, α' and may play a significant role for the transmission. Due to the strong molecule–electrode coupling the resonances originating from the molecular orbitals have weight inside the metal and mix with each other. The terms that describe the mixing are mainly positive leading to a lower sum of projected transmission. Occasionally they are negative which leads to a higher projected transmission at certain energies. The mixing can be quantified by the corresponding

[4] At some energies the sum of projected transmissions occasionally exceeds the total transmission, which is due to interference phenomena.

off-diagonal transmission,

$$T_{\alpha,\alpha'}(E) = \mathrm{Tr}\left[G(E)\Gamma_{\mathrm{L}}^{\alpha}(E)G^{\dagger}(E)\Gamma_{\mathrm{R}}^{\alpha'}(E)\right], \qquad (3)$$

where α and α' are different. In figure 7 we show the transmission for the LUMO and the LUMO+1 with (full lines) and without (dashed lines) the mixing with nearby orbitals including HOMO, LUMO, LUMO+1. Including the mixing yields a significant contribution and thus mixing between orbitals due to the strong coupling in the junction plays a significant role. Thus we conclude that the approximation of parallel transport through individual C_{60}-states neglects significant contributions to the conductance.

5. Conclusion

Conductance spectroscopy and first-principles transport calculations clarify the role molecular orbital resonances play in determining the conductance of a molecular junction at contact. A picture of electron transport through individual orbitals [2, 37] does not hold. Rather, for strong molecule–electrode couplings mixing of orbitals must be considered for the correct description of the junction conduction.

Acknowledgments

Financial support by the Deutsche Forschungsgemeinschaft through SFB 677 is acknowledged. We thank T Frederiksen (San Sebastian) for useful comments and the DCSC for computational resources.

References

[1] Landauer R 1970 *Phil. Mag.* **21** 863
[2] Scheer E, Agraït N, Cuevas J C, Yeyati A L, Ludoph B, Martín-Rodero A, Bollinger G R, van Ruitenbeek J M and Urbina C 1998 *Nature* **394** 154
[3] Brandbyge M, Kobayashi N and Tsukada M 1999 *Phys. Rev.* B **60** 17064
[4] Pauly F, Viljas J K, Huniar U, Häfner M, Wohlthat S, Bürkle M, Cuevas J C and Schön G 2008 *New J. Phys.* **10** 125019
[5] Bilan S, Zotti L A, Pauly F and Cuevas J C 2012 *Phys. Rev.* B **85** 205403
[6] Scheer E, Joyez P, Esteve D, Urbina C and Devoret M H 1997 *Phys. Rev. Lett.* **78** 3535
[7] Naaman O and Dynes R C 2004 *Solid State Commun.* **129** 299
[8] Agraït N, Untiedt C, Rubio-Bollinger G and Vieira S 2002 *Phys. Rev. Lett.* **88** 216803
[9] Néel N, Kröger J, Berndt R and Pehlke E 2008 *Phys. Rev.* B **78** 233402
[10] Vitali L, Ohmann R, Stepanow S, Gambardella P, Tao K, Huang R, Stepanyuk V S, Bruno P and Kern K 2008 *Phys. Rev. Lett.* **101** 216802
[11] Calvo M R, Fernandez-Rossier J, Palacios J J, Jacob D, Natelson D and Untiedt C 2009 *Nature* **458** 1150
[12] Néel N, Kröger J and Berndt R 2010 *Phys. Rev.* B **82** 233401
[13] Bork J, Zhang Y H, Diekhöner L, Borda L, Simon P, Kroha J, Wahl P and Kern K 2011 *Nat. Phys.* **7** 901
[14] Choi D J, Rastei M V, Simon P and Limot L 2012 *Phys. Rev. Lett.* **108** 266803
[15] Paulsson M and Brandbyge M 2007 *Phys. Rev.* B **76** 115117
[16] Néel N, Kröger J, Limot L, Frederiksen T, Brandbyge M and Berndt R 2007 *Phys. Rev. Lett.* **98** 065502
[17] Schulze G *et al* 2008 *Phys. Rev. Lett.* **100** 136801
[18] Néel N, Kröger J and Berndt R 2011 *Nano Lett.* **11** 3593
[19] Ulstrup S, Frederiksen T and Brandbyge M 2012 *Phys. Rev.* B **86** 245417
[20] Kiguchi M, Tal O, Wohlthat S, Pauly F, Krieger M, Djukic D, Cuevas J C and van Ruitenbeek J M 2008 *Phys. Rev. Lett.* **101** 046801
[21] Chen W, Widawsky J R, Vázquez H, Schneebeli S T, Hybertsen M S, Breslow R and Venkataraman L 2011 *J. Am. Chem. Soc.* **133** 17160–3
[22] Pai W W *et al* 2010 *Phys. Rev. Lett.* **104** 036103
[23] Perdew J P, Burke K and Ernzerhof M 1996 *Phys. Rev. Lett.* **77** 3865
[24] Soler J M, Artacho E, Gale J D, Garcia A, Junquera J, Ordejón P and Sánchez-Portal D 2002 *J. Phys.: Condens. Matter* **14** 2745
[25] Kresse G and Furthmüller J 1996 *Phys. Rev.* B **54** 11169
[26] Brandbyge M, Mozos J L, Ordejón P, Taylor J and Stokbro K 2002 *Phys. Rev.* B **65** 165401
[27] Abel M, Dimitriev A, Fasel R, Lin N, Barth J V and Kern K 2003 *Phys. Rev.* B **67** 245407
[28] Néel N, Kröger J and Berndt R 2008 *Nano Lett.* **8** 1219
[29] Néel N, Limot L, Kröger J and Berndt R 2008 *Phys. Rev.* B **77** 125431
[30] Schull G, Néel N, Becker M, Kröger J and Berndt R 2008 *New J. Phys.* **10** 065012
[31] Kröger J, Néel N and Limot L 2008 *J. Phys.: Condens. Matter* **20** 223001
[32] Wang L L and Cheng H P 2004 *Phys. Rev.* B **69** 045404
[33] Sanville E, Tang W and Henkelman G 2009 *J. Phys.: Condens. Matter* **21** 084204
[34] Grimme S 2006 *J. Comput. Chem.* **27** 1787
[35] Garcia-Lekue A and Wang L W 2010 *Phys. Rev.* B **82** 035410
[36] Stokbro K, Taylor J, Brandbyge M, Mozos J L and Ordejón P 2003 *Comput. Mater. Sci.* **27** 151–60
[37] Cuevas J C, Yeyati A L and Martín-Rodero A 1998 *Phys. Rev. Lett.* **80** 1066